Formation of supramolecular protein structures on gold surfaces

Running title: Protein structures on gold surfaces

Running Authors: Domigan et al.

Laura J. Domigan [a)]

The University of Auckland, School of Biological Sciences, Auckland 1010, New Zealand

Helen Ashmead

Callaghan Innovation, Lower Hutt, New Zealand

Simone Dimartino [a)]

The University of Edinburgh, Institute for Bioengineering, Edinburgh EH9 3BF, United Kingdom

Jenny Malmstrom [b)]

The University of Auckland, Department of Chemical and Materials Engineering, Auckland 1010, New Zealand

F. Grant Pearce [a)]

The University of Canterbury, School of Biological Sciences, Christchurch, New Zealand

Matthew Blunt [c)]

University College London, Department of Chemistry, United Kingdom

David E. Williams [b)]

The University of Auckland, Department of Chemistry, Auckland 1010, New Zealand

Juliet A. Gerrard [a), b), d)]

The University of Auckland, School of Biological Sciences and Department of Chemistry, Auckland 1010, New Zealand

[a)]Biomolecular Interaction Centre (BIC), New Zealand

[b)]The MacDiarmid Institute for Advanced Materials and Nanotechnology, New Zealand

[c)]email: m.blunt@ucl.ac.uk

[d)]email: j.gerrard@auckland.ac.nz

Recent research has highlighted the exciting possibilities enabled by the use of protein structures as nanocomponents to form functional nanodevices. To this end, control over protein-protein and protein-surface interactions is essential. In this study we probe the interaction of human peroxiredoxin 3 with gold surfaces, a protein that has been previously identified as having potential use in nanotechnology. Analytical ultracentrifugation and transmission electron microscopy revealed the pH mediated assembly of protein toroids into tubular structures across a small pH range. Quartz crystal microbalance with dissipation (QCM-D) measurements showed differences in absorbed protein mass when pH is switched from pH 8.0 to 7.2, in line with the formation of supramolecular structures observed in solution studies. Scanning tunneling microscopy (STM) under ambient conditions showed that these protein tubes form on surfaces in a concentration dependent manner, with a tendency for protein adsorption and supramolecular assembly at the edges of Au(111) terraces. Finally, SAM modification of Au surfaces was explored as a means to control the adsorption and orientation of pH triggered protein structures.

I. INTRODUCTION

There is a recognized role for biomolecular assemblies in nanotechnology, ranging from DNA origami through to supramolecular protein structures[1–4]. Proteins may be used as building blocks, or tectons, where their natural self-assembly properties are exploited to form valuable architectures. In addition, the diverse chemistry available through the polypeptide chain can be exploited to introduce non-native functionalities in these nanoconstructs[5–7]. The high degree of precision of protein assembly can also be used in a unique way to order other nanocomponents in multiple dimensions[1,8–10], such as

nanoparticle organization for plasmonic devices[11]. In the ordering of nanoscale building blocks for nanodevices such as bioelectronics and biomaterials, protein-surface interactions are an important consideration[12]. Gold surfaces are of particular interest as they can be readily modified via chemisorption of thiol containing compounds under ambient conditions, in order to create protein-reactive surfaces[13].

A number of challenges are associated with the control of supramolecular protein assemblies, in particular limitations to their manipulation outside of physiological conditions as well as their structural complexity[4]. Naturally occurring protein assemblies represent an ideal platform to overcome these limitations, enabling the investigation of the formation of these structures via environmental triggers[14,15]. The peroxiredoxin protein family can adopt a wide range of highly ordered quarternary structures, ranging from dimers and toroids[16,17], to stacks and tubes[15,18], catenanes[19] and, under certain conditions, cages[20]. Peroxiredoxins have a number of roles *in vivo*[21–25]. Their ability to function in multiple cellular roles is intrinsically linked to the oligomeric state of the protein[26]. The possibility of predicting conditions that initiate their controlled assembly makes this protein family particularly attractive as a novel protein tecton[10,15]. The peroxiredoxin family has been previously exploited for the formation of composite nanomaterials, such as binding of gold and palladium nanoparticles and to drive the stacking of graphene oxide layers[8].

In this study, we have used human peroxiredoxin III (*Hs*Prx3), which forms toroidal dodecamers comprising six oblique homodimers[27]. In the native protein, the switch between dimer and dodecamer occurs under non-reducing and reducing conditions respectively[15]. pH changes have an apparent effect on the oligomeric state of

peroxiredoxin[15], with wild type *Hs*Prx3 assembling into 1D tubes at pH 4.0[28]. In the current work we first assessed optimal conditions for the formation of high molecular weight species of the tagged human peroxiredoxin III (*Hs*Prx3-6his) using analytical ultracentrifugation (AUC) and transmission electron microscopy (TEM). The inclusion of a tag (which locates to the centre of the dodecameric ring) also provides a convenient method for metal binding through chelation to the 6 histidine residues[10,29,30].

This study reports the first findings of the surface assembly of *Hs*Prx3-6his. We investigated the interaction of *Hs*Prx3-6his with gold surfaces, with the goal of forming surface tethered supramolecular protein structures that could later be used for the formation of ordered nanoscale assembles. Scanning tunneling microscopy (STM) under ambient conditions enables the visualization of the morphology of surface immobilized proteins[31–36], and this, along with QCM-D, were used to monitor the absorption *Hs*Prx3-6his on gold surfaces. Self-assembled monolayers (SAMs) of functionalized thiols were used as a convenient method to create a protein platform[13].

II. EXPERIMENTAL

A. Protein expression and purification

The gene encoding *Hs*Prx3-6his, cloned into pET151-D-TOPO, was synthesized by Epoch Life Science. Chemically competent *E. coli* cells (BL21 (DE3) ROSETTA, Novagen 2013; genotype – F- *ompT hsds*B[B- mB-] *gal dcm* [DE3] pRARE [CamR]) were transformed with the plasmid via heat shock. The protein was successfully expressed in standard lysogeny broth (LB) media after shaking (180 rpm) at 37°C for 4 hours, in the presence of ampicillin and chloramphenicol, and then at 26°C, with the addition of isopropyl β-D-1thiogalactopyranoside (IPTG), for a further 20 hours. Cells

were lysed via sonication and the insoluble fraction was removed by centrifugation (18 000 x g, 30 minutes, 4 °C). *Hs*Prx2-6his was isolated from the soluble crude broth using IMAC and the sample was separated from any remained impurities using SEC.

B. Analytical ultracentrifugation (AUC)

Protein solutions were prepared at concentrations ranging from 0.15-0.6 mg/mL to a volume of 380 µL. Each sample was analysed with its own blank (400 µL) containing the corresponding buffer only. Quartz or sapphire cells were used with a path length of 1.2 cm. A wavelength scan was run prior to the experiment to determine the wavelength that provided the optimal optical density ($OD_{270\text{-}290}$ between 0.2 – 1.0). The centrifugal velocity was initially set at 38 000 rpm, with samples of a larger MW studied at 20 000 rpm to allow for sedimentation over a greater number of scans. All runs were completed at 20°C. The Svendberg sedimentation coeffient (S) was calculated using the c(s) model in SEDFIT. This software was also used to approximate particle mass using the below equation (**Equation 1**) [37]:

$$M = \frac{s \cdot f \cdot Na}{1 - \rho \cdot \bar{v}}$$

Equation 1. M = mass, s = sedimentation coefficient; f = frictional coefficient; Na = Avogadro's number; ρ = solvent density; $\bar{v}$ = partial specific volume

C. Transmission electron microscopy (TEM)

Protein samples were diluted to 50 µg/mL in dH_2O immediately prior to grid preparation. Carbon coated formvar 200-mesh copper grids were floated for 1 minute on 1) 20 µL protein sample; 2) 20 µL dH_2O (x3, 20 seconds each); 3) 1 % uranyl acetate negative stain. Excess dye was removed using fiber-less filter paper. Grids were then air-dried for

at least one hour before TEM analysis. Image collection was carried out on a FEI Morgagni 268D transmission electron microscope operating at 80 kV, with magnifications up to 180k. Images were captured using a SIS/Olympus Megapixel III digital camera mounted above the phosphor screen.

D. Quartz Crystal Microbalance with Dissipation (QCM-D)

Preparation of gold surfaces: Gold coated QCM-D crystals (Q-Sense, ATA Scientific, Tarren Point, NSW, Australia) with a fundamental frequency of 4.95 MHz were used. The gold sensors were cleaned with Piranha solution (5:1:1 Milli-Q water, ammonia (25 %), hydrogen peroxide (30 %)) at 75 °C for 10 min and then rinsed with hot Milli-Q water. The sensors were then dried under nitrogen and placed in an UV/ozone chamber (BioForce Nanosciences, USA) for 10 min.

QCM-D experiment: Protein adsorption onto gold surfaces was carried out using a QCM-D system (Q-sense E4 system, Biolin Scientific) equipped with a temperature controlled measuring chamber and a peristaltic pump (ISMATEC® IPC High Precision Multi channel Dispenser, IDEX Health and Science, Germany). Before each QCM-D experiment, pre-equilibrium with Milli-Q water and then the appropriate buffer was carried out for at least one hour, in order to reach a stable baseline before the addition of protein solutions. The test solutions were then introduced at a flow rate of 0.1 mL/min. All experiments were carried out at 22 °C.

E. Scanning Tunneling Microscopy (STM)

Preparation of gold surfaces: Au(111) substrates consisting of mica slides coated with 300 nm layer of Au metal were purchased from George Albert (BVD- Beschichtungen) and flame-annealed in a butane flame prior to use.

4-MBA SAM formation: Flame-annealed Au(111) substrates were immersed in 100 μM 4-MBA ethanolic solutions overnight. Substrates were then removed from solution, rinsed with solvent, dried under nitrogen. These surfaces were then exposed to protein samples.

NTA-thiol functionalisation: Flame-annealed Au(111) substrates were floated on a droplet of SH-NTA (1 mM in 100% ethanol) and incubated in an ethanol vapor chamber for 1.5 hours at room temperature. Following this, substrates were washed with 100% ethanol (5-10 min), 70% ethanol, milliQ H_2O (5-10 min), and the appropriate buffer solution (15 min). Surfaces were then incubated in 10 mM $NiCl_2$ (in buffer solution) for 15 min, followed by 2x buffer washes. These surfaces were then exposed to protein samples.

STM imaging: Protein samples were deposited onto Au(111) surfaces and allowed to adsorb, following by rinsing with appropriate buffer solutions and drying under nitrogen. For *in situ* adsorption studies a PTFE liquid cell was placed used and this was filled with the approximately 600 μL protein solution. STM experiments were carried out using a 5500 series SPM system (Keysight Technologies) operating under ambient conditions and at room temperature. STM tips were commercially purchased from Keysight technology and consisted of etched PtIr (80:20) tips coated in apiezon wax with only the tip apex exposed. Each tip was tested prior to use and had a guaranteed < 10 pA leakage current. All STM images were subject to a flattening process using the WSxM software package. No additional post processing has been applied to the images.

III. RESULTS AND DISCUSSION

A. HsPrx3 forms higher order structures in solution via a pH switch

Throughout this study, we have used an N-terminal his-tagged construct of human peroxiredoxin 3 (*Hs*Prx3-6his), with no tag cleavage following purification. Unlike the wild-type protein, the presence of an N-terminal histidine tag on *Hs*Prx3 generates a stable dodecamer in both reducing and non-reducing conditions, providing an ideal tecton from which larger structures can be formed (see Supporting Information, **Figure S1**). *Hs*Prx3-6his exists as a dodecameric toroid at pH 8.0, with an inner and outer diameter of 8 nm and 15 nm respectively, with the ring 4 nm in height (**Figure 1a**). We have found that in the presence of the N-terminal his-tag, the oligomerisation at pH 4.0 demonstrated by the wild-type protein is still present (see Supporting Information, **Figure S2**), but pH-triggered assembly and disassembly of stacked tubes also occurs over a more narrow pH range (pH 8.0-7.0), offering exciting prospects for the use of the switchable protein tecton over a physiological pH range. Size exclusion chromatography (SEC) showed that the switch between single rings and high molecular weight (HMW) oligomers occurs between pH 7.6 and 7.4 (see Supporting Information, **Figure S3**).

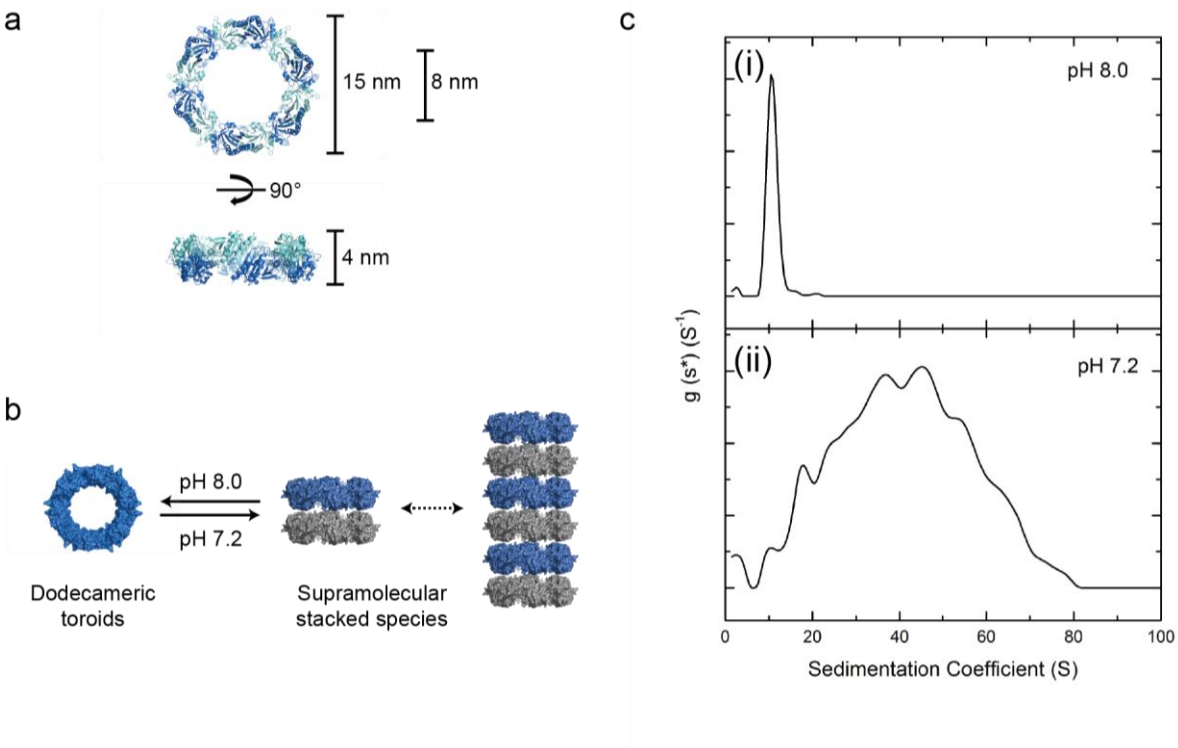

FIG. 1. **pH triggered assembly in solution.** (a) Structure of dodecameric *Hs*Prx3-6his with the monomers highlighted in alternate colours (blue and teal). (b) *Hs*Prx3-6his exists as a dodecameric torroid at pH 8.0, which self-associates to form stacked toroids at pH 7.2. (c) Analytical ultracentrifugation traces for *Hs*Prx3-6his at (i) pH 8.0, and (ii) pH 7.2.

Analytical ultracentrifugation

Assembly of *Hs*Prx3 in solution was investigated using analytical ultracentrifugation (AUC) across the pH range from pH 8.0-7.2 (see Supporting Information, **Figure S4**). At pH 8.0, there was a predominant species ~10.5 S (**Figure 1c, i**), close to the expected value for the *Hs*Prx3-6his dodecamer. There was also a small peak at ~2.5 S which is likely to represent the dimeric species. Decreasing the pH to 7.0 triggers the formation of a heterogeneous mixture of large oligomers, which is consistent with the rings stacking to form a tube (**Figure 1c, ii**).

As with the SEC results, the AUC data (**Figure S4**) also showed that small changes in pH had a large effect on the oligomeric state of *Hs*Prx3-6his, with the shift mainly located between pH 7.6 and 7.4. This level of control has not been seen previously for peroxiredoxins.

Transmission electron microscopy

Images captured using transmission electron microscopy (TEM) are in agreement with the solution data. *Hs*Prx3-6his at pH 8.0 is present as single rings (**Figure 2a**), but the degree of oligomerisation increases with decreasing pH, with the switch from rings to stacks to tubes occurring between pH 7.6 and 7.4 (see Supporting Information, **Figure S5**). At pH 7.2 the population is much more heterogeneous, with stacks of two and more present throughout the sample (**Figure 2b**), and tube size ranging from approximately 10 – 450 nm in length (stacks of 2-112 dodecamers).

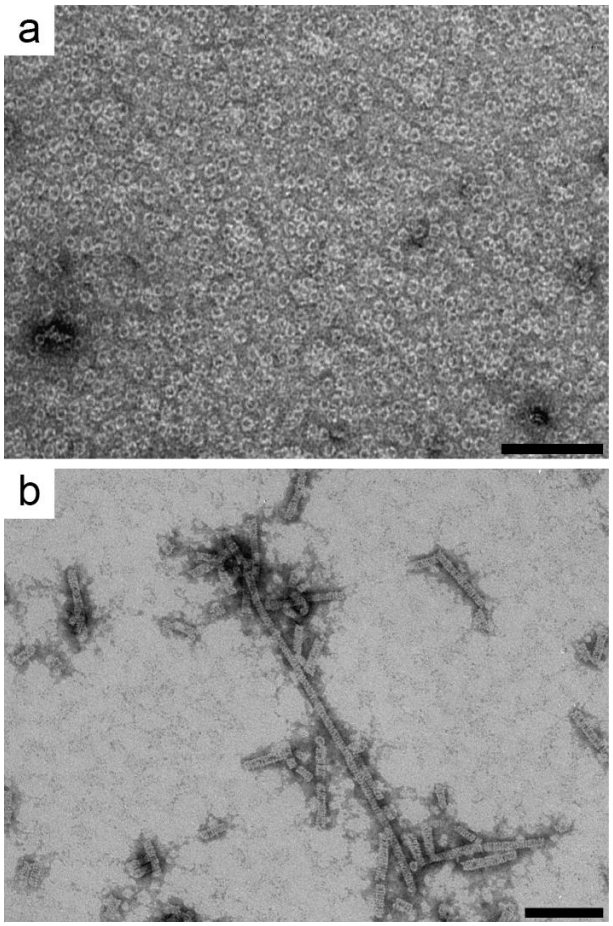

FIG. 2. **TEM imaging of *Hs*Prx3-6his.** Representative TEM images of *Hs*Prx3-6his at a) pH 8.0, and b) pH 7.2. Scale bars are 100 nm.

B. Assembly of HsPrx3-6his on gold surfaces

The interaction of *Hs*Prx3-6his with surfaces and surface-based formation of supramolecular protein structures was investigated using gold as a model surface. For surface assembly studies, we focused on the pH mediated switch between a homogenous population of single rings (pH 8.0), to the assembly of these rings into HMW species including stacked tubes. HMW assembly was monitored at pH 7.2 due to the population of single rings being unfavorable at this pH. (**Figure 1b**).

Quartz-crystal microbalance with dissipation (QCM-D)

Real-time monitoring of peroxiredoxin adsorption on gold surfaces was carried out via QCM-D. The time-course of a typical adsorption experiment on gold-coated sensors is shown in Figure 3. An initial equilibrium step was carried out in the appropriate buffer (pH 8.0 or pH 7.2) to establish a stable baseline. Solutions containing *Hs*Prx3-6his were then introduced into the system until stable frequency and dissipation signals were obtained. Following this, the sensors were washed with buffer and desorption monitored. The results obtained indicate rapid adsorption of *Hs*Prx3-6his onto gold surfaces. After injection, there was an immediate sharp decrease in the resonance frequency of the QCM sensor, accompanied by a slight increase in dissipation (**Figure 3**). Only a small frequency shift is observed following washing of the QCM sensor with buffer. These observations indicate that the protein adsorbs tightly to the underlying gold surface, forming a rigidly bound protein layer.

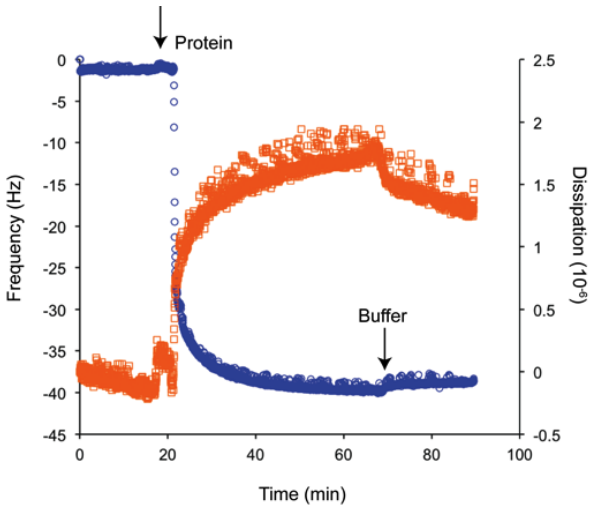

FIG. 3. **Representative traces of QCM-D raw data.** Frequency (left axis; blue trace) and dissipation (right axis; orange trace) for the 9th overtone of the QCM resonator for *Hs*Prx3-6his adsorption (pH 8.0, 0.1 mg/mL) on Au surface. The first arrow indicates

where protein is introduced to the system (following equilibration with buffer) and the second arrow indicates where the buffer wash step commences.

A greater adsorbed mass (i.e. greater frequency shift) was measured for pH 7.2 than pH 8.0 at a fixed protein concentration of 10 μg/mL (**Figure 4, i**), as expected due to the presence of HMW species at pH 7.2 and the formation of a thicker layer. At pH 8.0, where there is a single homogenous population of toroids, there is no observed concentration dependence of Δf (Supporting Information, Figure S6). This suggests xthe formation of a protein monolayer, which is independent of the concentration used, indicating the strong adsorption bonds between the gold surface and the protein molecules at pH 8.0. At pH 7.2 there is an increase in the mass adsorbed when protein concentration is increased to 100 μg/mL (Supporting Information, Figure S6). This is due to the concentration dependence of the equilibrium between heterogeneous species in solution, with increased protein concentration favoring the formation of higher order species, and therefore greater adsorbed mass.

The QCM data is also reported in terms of ΔD vs Δf. Distinctly different curves are apparent at pH 8.0 and 7.2 (**Figure 4,** ii, iii). At pH 8.0, the slope is relatively constant throughout the experiment, indicating that adsorption of the protein in its dodecameric form follows a similar mechanism, irrespective of the current surface coverage, leading to the formation of a rigid monolayer. At pH 7.2 there is an increased slope and two distinct phases, consistent with a rearrangement of the adsorbed stacks and change in their orientation during adsorption, thus facilitating further adsorption of *Hs*Prx3-6his tubes. This supports our hypothesis that the concentration dependent oligomerisation seen at this pH is also coupled to a rearrangement of protein molecules on the surface.

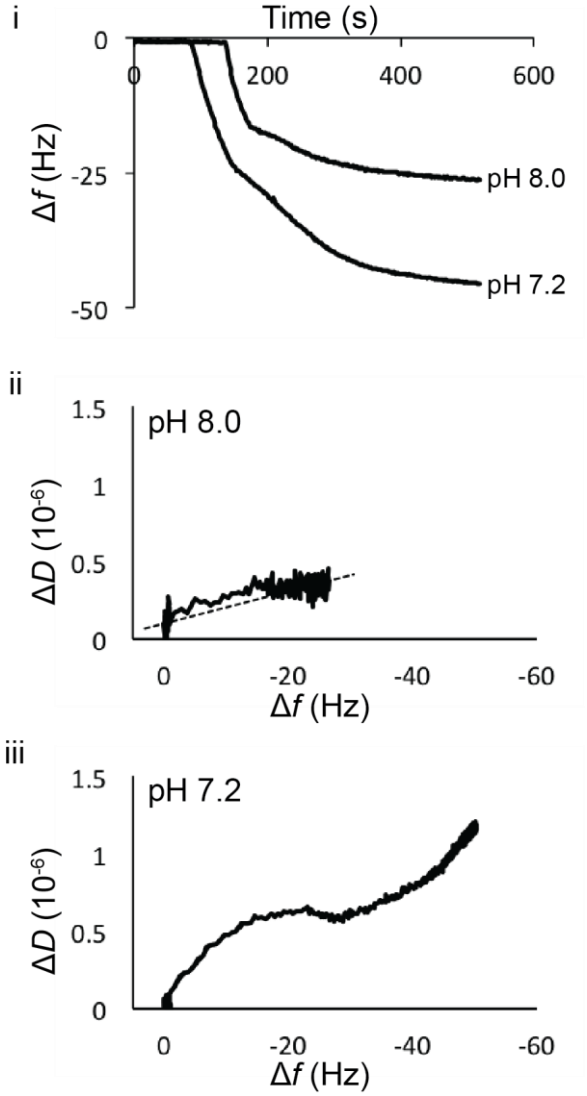

FIG. 4. Plots of QCM-D data for the adsorption of *Hs*Prx3-6his onto unmodified gold surfaces at pH 8.0 and pH 7.2 (10 μg/mL in appropriate buffer). (i) Representative time-course of Δ*f* for HsPrx3-6his adsorption at pH 8.0 and pH 7.2. Representative plots of Δ*D* vs Δ*f* obtained via QCM-D for the adsorption of HsPrx3 onto gold surfaces at (ii) pH 8.0 (dashed line is linear fit, $r^2 = 0.844$), and (iii) pH 7.2.

C. Scanning tunneling microscopy (STM)

The formation of high molecular weight species at pH 7.2 was further investigated using STM under ambient conditions. *Hs*Prx3-6his was purified at pH 8.0 and dialysed overnight at 4°C into pH 7.2 buffer, as prepared for solution studies. Following this, 10 μL of protein solution was deposited on flame annealed Au(111) on mica substrates and allowed to absorb for 10 min, followed by rinsing with buffer and H_2O. STM imaging was carried out under ambient air conditions at the solid-air interface, with images shown in Figure 5. Representative images obtained at low (5 μg/mL; **Figure 5A**) and high (50 μg/mL; **Figure 5B**) protein concentration demonstrate concentration dependent protein oligomerisation on surfaces. The images captured show a typical atomically flat area, with the naturally occurring terraces of the Au(111) surface..

At low concentration, *Hs*Prx3-6his was visible as discrete "globules" (**Figure 5A**, a and b), with line profiles showing dimensions of approximately 15 nm diameter and 0.5 nm height (**Figure 5A**, a-i, b-i,ii). This corresponds well to the dimensions of the crystal structure of *Hs*Prx3-6his (PDB 5JCG)[27], when consideration is given for the characteristic decrease in protein heights as measured by STM[38]. This is due to the conductivity of hydrated protein molecules being considerably less than that of the bare gold surface. The theoretical thickness of a dodecamer is 4 nm; STM indicates 0.4 nm so there is an approximate 10x reduction in the size (Figure 5A, a-i). An overlay of line profiles acquired from a number of protein molecules (Figure 5A, b-ii), confirms the dimensions to be representative of *Hs*Prx-6his dodecameric rings adsorbed flat on the Au(111) surface (see schematic; **Figure 5C, a**).

At increased protein concentration, association of peroxiredoxin rings into stacks and tubes is observed (**Figure 5B**, a and b). This is predominantly seen to occur at step edges

on the Au(111) surface. Line profiles show increased height (approximately 2 nm). If the approximate 10x reduction in height is accounted for this 20 nm could refer to either stacking of rings on the surface (Figure 5C, b), or lateral face-to-face association of *Hs*Prx3-6his rings (Figure 5C, c), similar to the structures observed via TEM imaging (Figure 2b). Line profiles of a tube and its cross-section support this hypothesis (Figure 5B, b-i, ii). Full monolayer coverage was not obtained due to the small volume and time allowed for protein adsorption, necessary to obtain images of individual protein molecules.

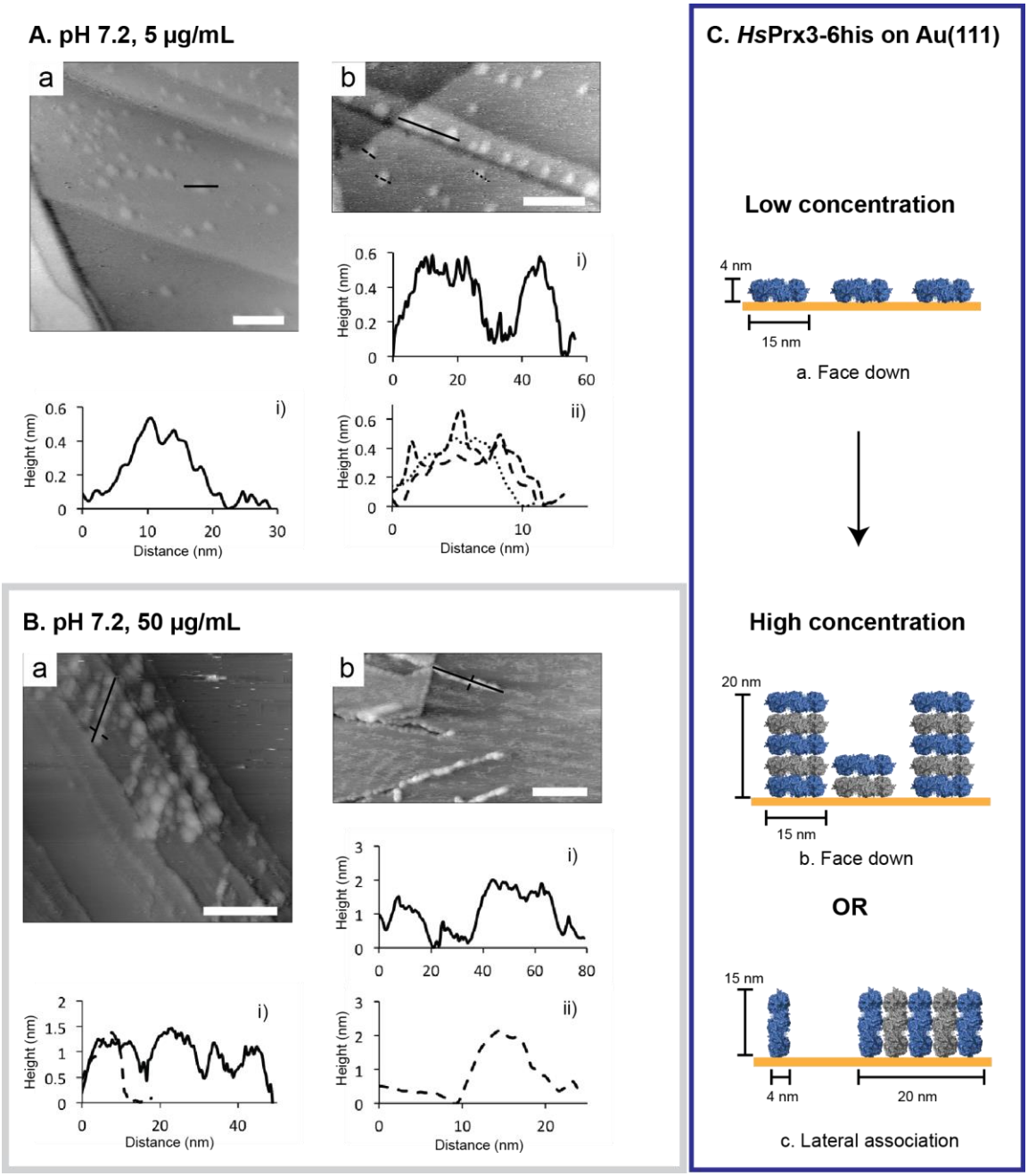

FIG. 5. **Assembly of *Hs*Prx3-6his tubes on Au surfaces.** STM images obtained of *Hs*Prx3-6his (pH 7.2) adsorbed on Au(111) surfaces. Representative STM images obtained at (A) low (5 µg/mL), and (B) high (50 µg/mL) protein concentration. Line profiles correspond to height as a function of distance for the areas indicated in the STM images. Dotted line profiles were taken perpendicular to the solid line profile (C) Schematic showing the proposed morphology of the adsorbed protein on the gold surface,

with concentration dependent protein oligomerisation (scale bars 50 nm). Dimensions are taken from the *Hs*Prx3 crystal structure (PDB 5JCG).

D. Controlling the adsorption and orientation of HsPrx3-6his on gold surfaces

The current use of peroxiredoxin as a tecton for the construction of surface nanodevices is limited by a lack of control over its orientation upon adsorption. We seek to form a uniform layer of protein stacks on surfaces, preferably with the central cavity exposed for accessibility to functional cargo into the ring cavity, such as metallic nanoparticles[10].

Towards this goal, Au surfaces were modified with self-assembled monolayers (SAMs) to investigate methods to control the adsorption and orientation of *Hs*Prx3-6his on Au surfaces.

SAM formation on gold surfaces

Au was modified with (i) 4-mercaptobenzoic acid (4-MBA) and (ii) nitrilotriacetic acid (NTA)-thiol conjugated to Ni^{2+} ions (see Supporting Information (**Figure S7**)). 4-MBA forms well characterised SAMs on gold surfaces[39]. Formation upon Au surfaces results in a protein reactive surface due to the presence of free carboxy groups that interact with available amines on the protein surface (Figure S7), with amide bond formation in the presence of EDC-NHS.

NTA-thiol SAM formation results in the surface availability of a NTA group, which forms a tetravalent chelate with Ni^{2+}. His-tagged proteins, such as the *Hs*Prx3-6his construct used in this study, bind via the interaction of histidine with surface immobilized Ni^{2+} ions, similar to the interactions used in immobilized metal affinity chromatography

(IMAC). This method results in the formation of a semi-permanent protein layer, which can be removed via displacement with metal ions or imidazole. The above SAMs were successfully formed on Au(111) surfaces and imaged using STM (**Figure S8**).

Assembly of HsPrx3-6his on SAM modified surfaces

STM imaging of *Hs*Prx3-6his adsorbed on Au(111) surfaces modified with MBA SAMs showed a number of globules, representative of protein immobilized on the Au surface (**Figure 6A,** a). The lack of movement of the globules with repeated scanning indicated that they were covalently bound (via EDC-NHS) to the surface, and the presence of the cross-linker appears to give better dispersion of the protein on the surface[40]. Line profiles show discrete globules to have dimensions of approximately 15 nm diameter and heights ranging from 0.5-2.4 nm, indicative of peroxiredoxin rings bound face down on the surface (Figure 6A, a-ii). In some images it was possible to visualize the central hole, supporting the above hypothesis (Figure 6A, a-ii). *Hs*Prx3-6his will covalently bind to the MBA surface via EDC-NHS mediated amide bond formation predominantly utilising surface accessible lysine residues, of which there are a number on the ring top and base (**Figure S7**). Based on dimensions measured for single rings (0.4 nm height; Figure 5), it appears that *Hs*Prx3-6his is predominantly bound face down on the surface with vertical stacking occurring, consisting of approximately one to six laterally associating protein rings.

To promote further stacking of peroxiredoxin rings, Au substrates "preseeded" with pH 7.2 *Hs*Prx3-6his, as described above, were then exposed to pH 4.0 HsPrx3-6his (Figure 6A, b). At pH 4.0 amide bond formation is less favourable and the formation of *Hs*Prx3-6his stacks is promoted (Figure S2). Histograms of height constructed from particle

analysis carried out on STM images show that this strategy resulted in the increased growth of protein columns on the surface (up to 4 nm in height) (Figure 6A, b-iii), compared to 2 nm stacks for those surfaces only exposed to the pH 7.2 protein (Figure 6A, a-iii).

Another strategy employed to immobilize peroxiredoxin stacks was via nickel complexed NTA-thiol SAMs. This also resulted in *Hs*Prx3-6his immobilisation, via interaction with the his-tag in the central ring cavity. In this case, discrete protein globules were also visualised (Figure 6B, i). Under these conditions there appeared to be less bound protein and for it to predominantly exist as single rings (Figure 6B, ii), with histograms showing limited stack formation (Figure 6B, iii). Based on our hypothesis that the his-tag mediates stacking at pH 7.2, we think this is due to competing interactions between his-tags on adjacent dodecamers, and the his-tag with the surface immobilized nickel. However, as mentioned previously, this immobilisation strategy results in a semi-permanent protein layer, with bound peroxiredoxin rings able to be displaced by high imidazole concentrations. This property could be exploited in later studies, or binding efficiency improved through chelation of cobalt in place of nickel [41].

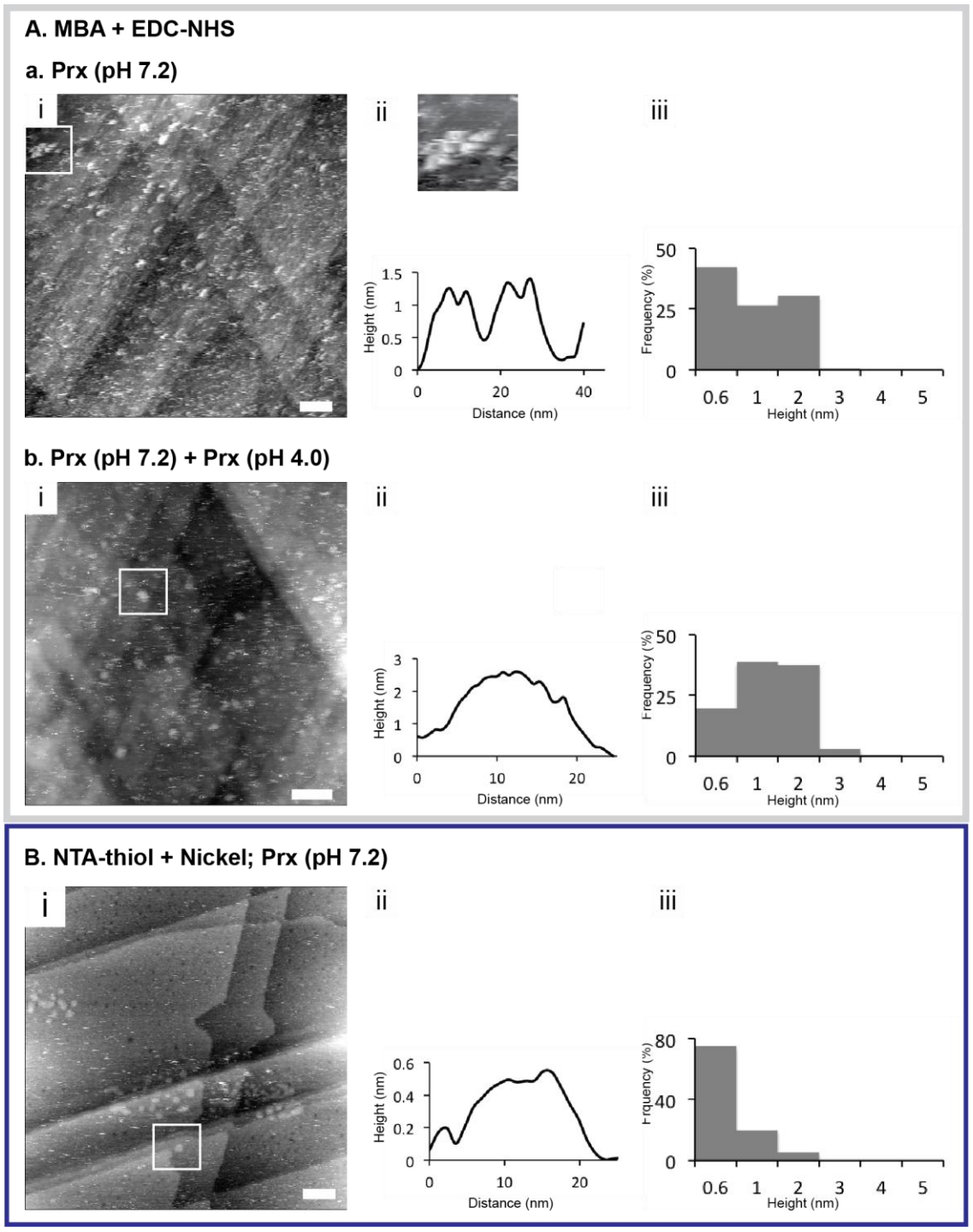

FIG. 6. **SAM mediated assembly of *Hs*Prx3-6his stacks.** Peroxiredoxin stacks were formed on Au(111) surfaces via immobilization of *Hs*Prx3-6his (pH 7.2) to SAMs formed from (A) MBA (in the presence of EDC-NHS), and (B) NTA-thiol (complexed to nickel). (i) Representative STM images of surface immobilized *Hs*Prx3-6his (scale bars

50nm). (ii) Line profiles corresponding to height as a function of distance for the areas indicated in the STM images. (iii) Histograms of HsPrx3-6his stack height from particle analysis of STM images.

IV. SUMMARY AND CONCLUSIONS

*Hs*Prx3 with a his-tag (*Hs*Prx3-6his) was shown via AUC and TEM to assemble into stacked toroids over a narrow physiological pH range (pH 7.2 – 8.0), in contrast to the untagged protein that forms tubes at pH 4.0. While the exact mode of oligomerisation is at this stage unclear, control over high molecular weight assembly of *Hs*Prx3-6his through small changes in pH places this protein as an ideal tecton for the formation of biological nanomaterials.

Having gained control of assembly in solution we are beginning to develop strategies to create organized 2D structures on surfaces. Non-specific protein adsorption on surfaces can lead to protein unfolding and desorption over time. Coupling via functional groups (such as amines and thiols), present at exposed surface amino acid residues, provides an easy method of surface immobilisation. However, even such coupling usually results in unspecific binding and random protein orientation at the interface. Specific binding interactions, such as biotin-strepavidin, or through incorporation of un-natural amino acids and purification tags, provide a means by which protein-surface interactions can be predicted and to some extent controlled, and generally lead to minimal protein denaturation upon adsorption [42–46].

Investigation into the assembly of *Hs*Prx3-6his on Au surfaces showed pH triggered supramolecular structures also formed on surfaces, as monitored by ambient STM and QCM-D. SAM modification (4-MBA and NTA-thiol chelated Ni^{2+}) of Au surfaces was used as a means to control the adsorption and orientation of protein tubes on surfaces.

This presents the first critical step in surface assembly of this protein tecton, towards its use for the ordering of nanocomponents.

ACKNOWLEDGMENTS

This work was funded by The MacDiarmid Institute for Advanced Materials and Nanotechnology, and Callaghan Innovation Ltd.

1. Medalsy, I. *et al.* SP1 protein-based nanostructures and arrays. *Nano Lett.* **8,** 473–477 (2008).
2. Douglas, S. M. *et al.* Self-assembly of DNA into nanoscale three-dimensional shapes. *Nature* **459,** 414–418 (2009).
3. Rothemund, P. W. K. Folding DNA to create nanoscale shapes and patterns. *Nature* **440,** 297–302 (2006).
4. Kim, Y. & Jung, Y. Artificial supramolecular protein assemblies as functional high-order protein scaffolds. *Org. Biomol. Chem.* (2016). doi:10.1039/C6OB00116E
5. Inaba, H. *et al.* A metal carbonyl-protein needle composite designed for intracellular CO delivery to modulate NF-kappa B activity. *Mol. Biosyst.* **11,** 3111–3118 (2015).
6. Kim, Y. E., Kim, Y., Kim, J. A., Kim, H. M. & Jung, Y. Green fluorescent protein nanopolygons as monodisperse supramolecular assemblies of functional proteins with defined valency. *Nat Commun* **6,** 7134 (2015).
7. Sun, H. *et al.* Micelle-Induced Self-Assembling Protein Nanowires: Versatile Supramolecular Scaffolds for Designing the Light-Harvesting System. *ACS Nano* **10,** 421–428 (2016).
8. Ardini, M. *et al.* Supramolecular self-assembly of graphene oxide and metal nanoparticles into stacked multilayers by means of a multitasking protein ring. *Nanoscale* **8,** 6739–6753 (2016).
9. Malmstroem, J. *et al.* Protein nanorings organized by poly(styrene-block-ethylene oxide) self-assembled thin films. *Nanoscale* **7,** 19940–19948 (2015).

10. Ardini, M. *et al.* Metal-induced self-assembly of peroxiredoxin as a tool for sorting ultrasmall gold nanoparticles into one-dimensional clusters. *Nanoscale* **6,** 8052–8061 (2014).
11. Hoeller, R. P. M. *et al.* Protein-Assisted Assembly of Modular 3D Plasmonic Raspberry-like Core/Satellite Nanoclusters: Correlation of Structure and Optical Properties. *ACS Nano* **10,** 5740–5750 (2016).
12. Zaitouna, A. J. & Lai, R. Y. An electrochemical peptide-based Ara h 2 antibody sensor fabricated on a nickel(II)-nitriloacetic acid self-assembled monolayer using a His-tagged peptide. *Anal. Chim. Acta* **828,** 85–91 (2014).
13. Whitesides, G. M., Mathias, J. P. & Seto, C. T. Molecular self-assembly and nanochemistry: A chemical strategy for the synthesis of nanostructures. *Science* **254,** 1312–1319 (1991).
14. Ashmead, H. M., Negron, L., Webster, K., Arcus, V. & Gerrard, J. A. Proteins as Supramolecular Building Blocks: Nterm-Lsr2 as a New Protein Tecton. *Biopolymers* **103,** 260–270 (2015).
15. Phillips, A. J. *et al.* Peroxiredoxin is a Versatile Self-Assembling Tecton for Protein Nanotechnology. *Biomacromolecules* **15,** 1871–1881 (2014).
16. Hall, A., Karplus, P. A. & Poole, L. B. Typical 2-Cys peroxiredoxins - structures, mechanisms and functions. *FEBS J.* **276,** 2469–2477 (2009).
17. Wood, Z. A., Poole, L. B., Hantgan, R. R. & Karplus, P. A. Dimers to doughnuts: Redox-sensitive oligomerization of 2-cysteine peroxiredoxins. *Biochemistry* **41,** 5493–5504 (2002).

18. Saccoccia, F. *et al.* Moonlighting by Different Stressors: Crystal Structure of the Chaperone Species of a 2-Cys Peroxiredoxin. *Structure* **20,** 429–439 (2012).
19. Cao, Z., McGow, D. P., Shepherd, C. & Lindsay, J. G. Improved Catenated Structures of Bovine Peroxiredoxin III F190L Reveal Details of Ring-Ring Interactions and a Novel Conformational State. *PLoS One* **10,** e0123303 (2015).
20. Meissner, U., Schroder, E., Scheffler, D., Martin, A. G. & Harris, J. R. Formation, TEM study and 3D reconstruction of the human erythrocyte peroxiredoxin-2 dodecahedral higher-order assembly. *Micron* **38,** 29–39 (2007).
21. Karplus, P. A. A primer on peroxiredoxin biochemistry. *Free Radic. Biol. Med.* **80,** 183–190 (2015).
22. Perkins, A., Nelson, K. J., Parsonage, D., Poole, L. B. & Karplus, P. A. Peroxiredoxins: guardians against oxidative stress and modulators of peroxide signaling. *Trends Biochem.Sci.* **40,** 435–445 (2015).
23. Banerjee, M., Chakravarty, D. & Ballal, A. Redox-dependent chaperone/peroxidase function of 2-Cys-Prx from the cyanobacterium Anabaena PCC7120: role in oxidative stress tolerance. *BMC plant biology* **15,** 444 (2015).
24. Cox, A. G., Winterbourn, C. C. & Hampton, M. B. Mitochondrial peroxiredoxin involvement in antioxidant defence and redox signalling. *Biochem. J.* **425,** 313–325 (2010).
25. Perkins, A., Poole, L. B. & Karplus, P. A. Tuning of Peroxiredoxin Catalysis for Various Physiological. *Biochemistry* **53,** 7693–7705 (2014).

26. Hall, A., Nelson, K., Poole, L. B. & Karplus, P. A. Structure-based Insights into the Catalytic Power and Conformational Dexterity of Peroxiredoxins. *Antioxid. Redox Signal.* **15,** 795–815 (2011).

27. Yewdall, N. A. *et al.* Structures of Human Peroxiredoxin 3 Suggest Self-Chaperoning Assembly that Maintains Catalytic State. *Structure* **24,** 1120–1129 (2016).

28. Radjainia, M. *et al.* Cryo-Electron Microscopy Structure of Human Peroxiredoxin-3 Filament Reveals the Assembly of a Putative Chaperone. *Structure* **23,** 912–920 (2015).

29. Ferrer-Miralles, N. *et al.* Biological activities of histidine-rich peptides; merging biotechnology and nanomedicine. *Microb. Cell. Fact.* **10,** 101 (2011).

30. Wegner, S. V., Schenk, F. C. & Spatz, J. P. Cobalt(III)-Mediated Permanent and Stable Immobilization of Histidine-Tagged Proteins on NTA-Functionalized Surfaces. *Chem.-Eur. J.* **22,** 3156–3162 (2016).

31. Contera, S. A., Iwasaki, H. & Suzuki, S. Ambient STM and in situ AFM study of nitrite reductase proteins adsorbed on gold and graphite: influence of the substrate on protein interactions. *Ultramicroscopy* **97,** 65–72 (2003).

32. Haggerty, L. & Lenhoff, A. Analysis of Ordered Arrays of Adsorbed Lysozyme by Scanning Tunneling Microscopy. *Biophys. J.* **64,** 886–895 (1993).

33. Kim, S.-U. *et al.* Direct immobilization of cupredoxin azurin modified by site-directed mutagenesis on gold surface. *Ultramicroscopy* **108,** 1390–1395 (2008).

34. Contera, S. A. & Iwasaki, H. Imaging the proteins pseudoazurin and apo-pseudoazurin on gold by STM in air: effect of the bias voltage. *Ultramicroscopy* **91,** 231–243 (2002).

35. Rzeznicka, I. I. *et al.* Observation of photoactive yellow protein anchored to a modified Au(111) surface by scanning tunneling microscopy. *Chem. Phys. Lett.* **472,** 113–117 (2009).

36. Raigoza, A. F., Dugger, J. W. & Webb, L. J. Review: Recent Advances and Current Challenges in Scanning Probe Microscopy of Biomolecular Surfaces and Interfaces. *ACS Appl. Mater. Interfaces* **5,** 9249–9261 (2013).

37. Schuck, P. Size-distribution analysis of macromolecules by sedimentation velocity ultracentrifugation and Lamm equation modeling. *Biophys. J.* **78,** 1606–1619 (2000).

38. Yusoff, H. M. *et al.* Excitation energy migration in yellow fluorescent protein (citrine) layers adsorbed on modified gold surfaces. *Appl. Surf. Sci.* **280,** 776–782 (2013).

39. Creager, S. & Steiger, C. Conformational Rigidity in a Self-Assembled Monolayer of 4-Mercaptobenzoic Acid on Gold. *Langmuir* **11,** 1852–1854 (1995).

40. Bedford, E. E., Boujday, S., Humblot, V., Gu, F. X. & Pradier, C.-M. Effect of SAM chain length and binding functions on protein adsorption: beta-Lactoglobulin and apo-transferrin on gold. *Colloid Surf. B-Biointerfaces* **116,** 489–496 (2014).

41. Wegner, S., Schenk, F. C. & Spatz, J. P. Cobalt(III) mediated permanent and stable immobilization of His-tagged proteins on NTA functionalized surfaces. *Chemistry – A European Journal* **22,** 3156–3162 (2016).

42. Young, J. F. *et al.* Strong and Reversible Monovalent Supramolecular Protein Immobilization. *ChemBioChem* **11,** 180–183 (2010).

43. Jonkheijm, P., Weinrich, D., Schroeder, H., Niemeyer, C. M. & Waldmann, H. Chemical Strategies for Generating Protein Biochips. *Angew. Chem.-Int. Edit.* **47,** 9618–9647 (2008).

44. Gonzalez-Campo, A. *et al.* Supramolecularly Oriented Immobilization of Proteins Using Cucurbit[8]uril. *Langmuir* **28,** 16364–16371 (2012).

45. Syguda, A. *et al.* Immobilization of Biotinylated hGBP1 in a Defined Orientation on Surfaces Is Crucial for Uniform Interaction with Analyte Proteins and Catalytic Activity. *Langmuir* **28,** 6411–6418 (2012).

46. Turchanin, A. *et al.* Molecular self-assembly, chemical lithography, and biochemical tweezers: A path for the fabrication of functional nanometer-scale protein arrays. *Adv. Mater.* **20,** 471–+ (2008).